The effect of fog on the probability density distribution of the ranging data of imaging laser radar

Wenhua Song, JianCheng Lai, Zabih Ghassemlooy, Zhiyong Gu, Wei Yan, Chunyong Wang, and Zhenhua Li

Citation: AIP Advances **8**, 025022 (2018); doi: 10.1063/1.5011781
View online: https://doi.org/10.1063/1.5011781
View Table of Contents: http://aip.scitation.org/toc/adv/8/2
Published by the American Institute of Physics

The effect of fog on the probability density distribution of the ranging data of imaging laser radar

Wenhua Song,[1] JianCheng Lai,[1,a] Zabih Ghassemlooy,[2,3] Zhiyong Gu,[1] Wei Yan,[1] Chunyong Wang,[1] and Zhenhua Li[1]

[1]*Information Physics and Engineering, Nanjing University of Science and Technology, Nanjing, Jiangsu 210094, China*

[2]*Optical Communications Research Group, NCRLab, Faculty of Engineering & Environment, University of Northumbria at Newcastle, Newcastle upon Tyne NE1 8ST, UK*

[3]*QIEM, Haixi Institutes, Chinese Academy of Sciences, Qianzhou, Fujian 350002, China*

(Received 3 November 2017; accepted 19 February 2018; published online 28 February 2018)

This paper outlines theoretically investigations of the probability density distribution (PDD) of ranging data for the imaging laser radar (ILR) system operating at a wavelength of 905 nm under the fog condition. Based on the physical model of the reflected laser pulses from a standard Lambertian target, a theoretical approximate model of PDD of the ranging data is developed under different fog concentrations, which offer improved precision target ranging and imaging. An experimental test bed for the ILR system is developed and its performance is evaluated using a dedicated indoor atmospheric chamber under homogeneously controlled fog conditions. We show that the measured results are in good agreement with both the accurate and approximate models within a given margin of error of less than 1%.
https://doi.org/10.1063/1.5011781

I. INTRODUCTION

Over the past few decades, laser radar systems (or imaging laser radar (ILR)) with high-resolution three-dimensional (3-D) images[1] have become an attractive option for range finding in a number of applications including target recognition, space exploration, obstacle avoidance to name a few.[2–5] However, in outdoor environments ILR systems performances are highly dependent on the weather conditions such as fog, rain, snow, pollution, and turbulence, which need further investigations. Recent studies have shown that the optical power loss for the dense maritime fog and moderate continental fog can be as high as 480 dB/km and 120 dB/km, respectively thus reducing the link visibility to less than 100 meters.[6,7] For more on fog and a range of models that have been developed the readers are referred to[8–14] the references within. In time-of-flight ILR systems, the target range is determined by measuring the time interval between the incident and reflected light (laser) pulses. In such systems, the reflected pulse can be used to trigger the time-digital convertor (TDC) module, thus avoiding the timing jitter at the start. Note that, for a highly accurate TDC the time precision is as low as sub-nanoseconds. For example, the TDC-GPX (by ACAM Inc.) has a timing precision of 75 ps full-width at half-maximum (FWHM) and the corresponding range precision is about 0.01 m. However, the range jitter is much higher than 0.1 m for ILR under low signal to noise ratio (SNR) levels.[15] Note that, the timing jitter is mainly due to identification of the reflected pulse, which can be affected by the weather conditions.

In this work, we investigate the influence of fog on the timing jitter (i.e., the probability density distribution (PDD) of the ranging data $d_{ra}(t)$) of ILR by means of peak-detecting identification. For a fixed target, range detection measurement, based on measuring the time-of-flight of the reflected

[a]Corresponding author. E-mail address: laijiancheng@njust.edu.cn

pulse, depends both on the channel condition (i.e., fog in this case) and the noise sources associated with ILR. In ILR systems, PDD of $d_{ra}(t)$ significantly influence the target recognition accuracy. In Ref. 16 an analytical model for the backscattered luminance with fog was proposed and an expression for the SNR as a function of meteorological visibility range based on the single scattering process was given. In Ref. 17 J. W. Giles, etc., presented an analytical model of a laser radar system by considering the presence aerosols within the propagation path, which accurately predicted the shape of the backscattered returned signals from the target. In Ref. 15 L. Jiancheng, etc., developed a stochastic model to derive the range uncertainty distribution of a peak detecting laser radar system. The analytical solution proposed was able to describe PDD of $d_{ra}(t)$ for a range of signal amplitudes, waveforms and noise sources. The results showed that PDD is proportional to both the 2nd derivative of the laser signal and the probability distribution of differential noise. In Ref. 18 S. Y. Chua, etc., theoretically and experimentally investigated the influence of target reflection on the 3-D range gated reconstruction. Based on laser detection and ranging (LADAR) and the bidirectional reflection distribution function theory, a 3-D range gated reconstruction model was developed and the target range accuracy was investigated by considering the incidence angle of the laser beam and the target surface reflectivity. In Ref. 19 C. Gröwall, etc., developed a time-of-flight radar simulator to study the influence of laser radar sensor parameters on the range statistical distribution. The authors concluded that the range uncertainty could be modeled as Gaussian (normal) distribution, given that there are differences between Gaussian fitting curves and the simulated statistical $d_{ra}(t)$. In Ref. 20 S. Johnson analyzed the probability density function (PDF) by considering both the local and global errors and showed that PDF is a function of SNR, range search interval and the level of speckle diversity.

To the best of our knowledge no works on the relationship between the characteristics of fog and PDD of $d_{ra}(t)$, which is important in characterizing the availability of ILR, have been reported. In this work, we have shown that the range of PDD is directly determined from the laser signal profile and by knowing the fog intensity. To this end, we have developed a theoretical model for PDD of $d_{ra}(t)$ under different fog conditions and show that the simulation results are in a good agreement with the predicted data. Considering the complexity of integral in the predicted model, an approximate model is proposed to determine PDD of $d_{ra}(t)$. To validate the concept, an experimental ILR system is developed and tested using a dedicated indoor atmospheric chamber under fog conditions. The measured results match quite well with both the accurate and approximate models within a given margin of errors less than 1%. The results reported can be used to offer a priori estimation of PDD of a laser radar system under fog conditions and improve the precision of target ranging and imaging.

The rest of this paper is organized as follows: section II describes details of the characteristics of the fog while section III focuses on the theoretical model of PDD of $d_{ra}(t)$. Section IV is all about the experiment setup for ILR with fog and in section V the experiment results and discussions are presented. Finally, the concluding remarks are presented in Section VI.

II. THE CHARACTERISTICS OF FOG

Fog droplet sizes can change very rapidly in both space and time under the influence of different physical processes, and its distribution is most crucial when determining its attenuation. Since the distribution of fog droplets is not easy to quantify, therefore a number of drop size distribution (DSD) based models have been proposed. The classical and widely used model is lognormal distribution, which is given by:[13,21,22]

$$n(r) = \frac{N_0}{\sqrt{2\pi}\ln\sigma_g r}\exp\left[-\frac{1}{2}\left(\frac{\ln(r/r_g)}{\ln\sigma_g}\right)^2\right], \tag{1}$$

where $n(r)$ is the volume concentration (m^{-3}), N_0 is the particle number density (m^{-3}), r is the particle size radius (μm), r_g is the distribution median radius, and σ_g is the geometric standard deviation.

The exact DSD of fog can be determined by knowing the values of r_g, σ_g, N_0, the effective radius of the distribution r_e and the liquid water content (LWC), which is proportional to the total volume of particles.

Note that, r_e is characterized as given by:[11]

$$r_e = \frac{\text{total volume}}{\text{total geom. cross section}} = \frac{\int_0^\infty r^3 n(r) dr}{\int_0^\infty r^2 n(r) dr}. \tag{2}$$

Substituting (1) into (2), we have:

$$r_e = r_g \exp\left[\frac{5}{2}(\ln \sigma_g)^2\right]. \tag{3}$$

The *LWC* is defined as:

$$LWC = \int_0^\infty \frac{4}{3}\pi r^3 \rho n(r) dr, \tag{4}$$

where ρ is the density of the fog droplet. Substituting (1) into (4), we obtain:

$$LWC = \frac{4}{3}\pi r_g^3 \rho N_0 \exp\left[\frac{9}{2}(\ln \sigma_g)^2\right]. \tag{5}$$

For fog particles, with the size in the order of the laser wavelength λ, Mie theory is applied as in Refs. 15 and 16, with the extinction coefficient is given by:[23,24]

$$\alpha_{ext} = \int_0^\infty C_{ext}(\frac{2\pi r}{\lambda}, n')n(r)dr, \tag{6}$$

where n' is the real part of the refractive index of water, C_{ext} is the droplet extinction cross section. However, C_{ext} weighted by DSD is not easy to be estimated. Note that, the total extinction due to fog particles in the atmosphere is the sum of absorption and scattering of light. For λ of 905 nm, which is adopted in this work, molecular absorption is considered to be negligible. Therefore, for the laser pulse α_{ext} can be estimated by the scattering of fog as given by:

$$\alpha_{ext} = \alpha_{sca} = \int_0^\infty C_{sca}(\frac{2\pi r}{\lambda}, n')n(r)dr, \tag{7}$$

where C_{sca} is the scatting cross section.

A propagating ray of light interacting with scattering particles (i.e., fog), will experience scattering in all directions. The intensity of scattered light will depend on the phase function of the particle, which is given by:

$$P(\theta) = \frac{4\pi N_0 S_{11}(\theta)}{(2\pi/\lambda)^2 \alpha_{sca}}, \tag{8}$$

where $S_{11}(\theta)$ is the first Mueller matrix element determined from Mie theory.

Based on the phase function, we can also obtain the backscattered coefficients of the fog (or air). Generally, due to the complex physical properties of fog its distribution is not readily available. Therefore, to predict the fog induced attenuation, where visibility V is used for characterization of fog, simple empirical fog models have been adopted, see Refs. 25–30 for more details.

III. MODELING OF PDD OF THE RANGING DATA

In an outdoor environment with fog, the reflected light (i.e., laser) power from a standard Lambertian target, which is larger than the arrived laser spot size, is given by:[4,16,31]

$$P_r(l)=\begin{cases}\dfrac{P_0\eta_e\eta_r O(l)\beta_{air}(\pi)\frac{c\tau_{\text{int}}}{2}\pi(\frac{D}{2})^2\exp(-2\int_0^l\alpha_{air}dl)}{l(l-\frac{c\tau_{\text{int}}}{2})} & l \text{ is before the fog}\\ \dfrac{P_0\eta_e\eta_r O(l)(\beta_{fog}(\pi)+\beta_{air}(\pi))\frac{c\tau_{\text{int}}}{2}\pi(\frac{D}{2})^2\exp(-2\int_0^l(\alpha_{ext}+\alpha_{air})dl)}{l(l-\frac{c\tau_{\text{int}}}{2})} & l \text{ is in the fog}\\ \dfrac{P_0\eta_e\eta_r O(l)\rho_t\pi(\frac{D}{2})^2\exp(-2\int_0^l(\alpha_{ext}+\alpha_{air})dl)}{l^2} & l \text{ is at the target}\end{cases}, \tag{9}$$

where P_0 is the initial transmit laser power, η_e and η_r are the transmittance of the laser beam at the source and receiver (Rx), respectively. $O(l)$ is the overlap function, $\beta_{fog}(\pi)$ and $\beta_{air}(\pi)$ are the volume backscattered coefficients of the fog and air, respectively. τ_{int} is the integration time of the lidar system, D is the aperture diameter of the Rx, α_{ext} and α_{air} are the extinction coefficients due to the fog and air, respectively. ρ_t is the hemispherical reflectance of the standard Lambertian target. c is the velocity of light and $l = ct/2$ is related to the flight time of optical pulse. Therefore, the time-resolved output of the lidar system without the noise is given by:

$$f(t)=K\int_0^t P_e(\tau)P_r(t-\tau)d\tau=KP_e(t)*P_r(t), \tag{10}$$

where K is a scaling constant, which is related to the responsivity of the photodetector and the electrical amplifier gain. $P_e(t)$ is the instrument impulse response function, which can be measured at the Rx with no fog. In the literatures, a number of functions have been used to describe $P_e(t)$ including Gauss function, parabolic function and Heavy-tailed function. Here, we determine PDD of $d_{ra}(t)$, which is obtained using the laser radar, and has a received pulse shape $y_r(t)$ defined as:

(i) The Gaussian function - most commonly used to describe $P_e(t)$ and is given by:[19]

$$P_e(t)=\frac{1}{\sqrt{2\pi}\tau}\exp\left[-\left(\frac{t-t_0}{\tau}\right)^2\right]. \tag{11}$$

(ii) The parabolic function - first proposed by Cain describes the laser echo pulse profile and is given by:[32]

$$P_e(t)=\left[1-\left(\frac{t-t_0}{\tau}\right)^2\right]rect\left(\frac{t-t_0}{\tau}\right). \tag{12}$$

(iii) Heavy-tailed function - introduced by Steinvall, which has a asymmetric profile with rapid rising and slow falling edges, and is given as:[33]

$$P_e(t)=\left(\frac{t-t_0}{\tau}\right)^2\exp\left(-\frac{t-t_0}{\tau}\right). \tag{13}$$

Fig. 1 is shows the received pulse with a FWHM of ~20 ns for three profiles defined in (11) to (13), with the peak at a flight time t_0 of 31.5 ns. Note that, the parameters adopted are the same as the experimental ILR system.

The received signal is given as:

$$S(t)=f(t)+n(t), \tag{14}$$

where $n(t)$ is the additive white Gaussian noise (AWGN). For a time-of-flight laser radar, every single range event is independent of each other. According to the central limit theorem, any point $s(t_k)$, which belongs to $S(t)$, obeys the normal distribution and is given by:[34]

$$g\left[s(t_k)\right]=\frac{1}{\sqrt{2\pi}\sigma_n}\exp\left\{-\frac{\left[s(t_k)-f(t_k)\right]^2}{2\sigma_n^2}\right\}, \tag{15}$$

where $f(t_k)$ and σ_n are the mean and standard deviation, respectively.

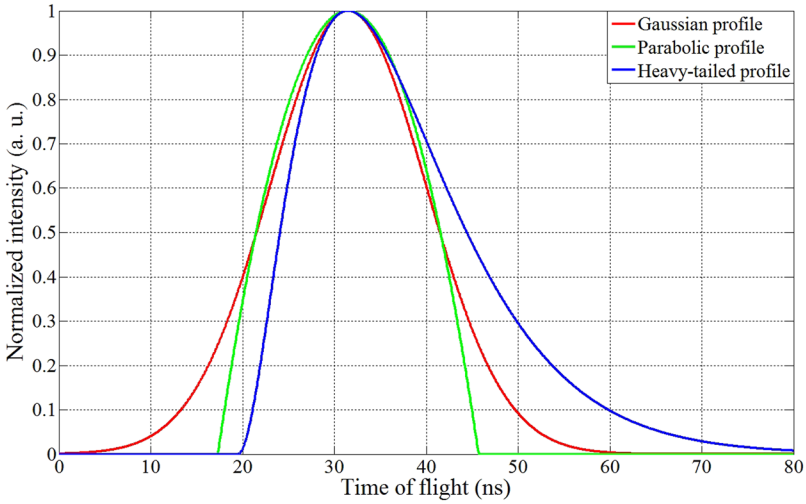

FIG. 1. The waveforms of received pulse for three profiles with the width of ~20ns.

For an imaging laser radar system with peak detection and a discrete sampling period T (with N number of total sampling points) using (14) and (15), the PDD model of the ranging data, which $s(t_k)$ is the maximum value of $S(t)$, can be expressed as:

$$\begin{aligned} p\left[S(t)_{\max} = s(t_k)\right] &= \sum_{s(t_k)=-\infty}^{s(t_k)=+\infty} g[s(t_k)] \prod_{i=1, i\neq k}^{i=N} \int_{-\infty}^{s(t_k)} g[S(t_i)] dS(t_i) \\ &= \sum_{s(t_k)=-\infty}^{s(t_k)=+\infty} g[s(t_k)] \exp\left[\sum_{i=1, i\neq k}^{i=N} \ln \int_{-\infty}^{s(t_k)} g\left[S(t_i)\right] dS(t_i)\right]. \end{aligned} \tag{16}$$

To simplify (16), the Gaussian error function is introduced to describe the cumulative PDF of Gaussian distribution as given by:

$$\begin{aligned} \Phi\left[s\left(t_k\right)\right] &= \int_{-\infty}^{s(t_k)} g[S(t_i)] dS(t_i) \\ &= \frac{1}{\sqrt{2\pi}\sigma_n} \int_{-\infty}^{s(t_k)} \exp\left\{-\frac{\left[s\left(t_k\right) - f\left(t_k\right)\right]^2}{2{\sigma_n}^2}\right\} ds\left(t_k\right). \\ &= \frac{1}{2}\left[1 + erf\left(\frac{s\left(t_k\right) - f\left(t_k\right)}{\sqrt{2}\sigma_n}\right)\right] \end{aligned} \tag{17}$$

Substituting (17) into (16) we obtain:

$$p\left[S(t)_{\max} = s\left(t_k\right)\right] = \int_{-\infty}^{+\infty} g\left[s\left(t_k\right)\right] \prod_{t_k=0}^{t_k=T} \Phi\left[s\left(t_k\right)\right] ds\left(t_k\right). \tag{18}$$

In order to verify the accuracy of the PDD model, we have simulated the range finding for 10,0000 times, which is equivalent to 10s of laser radar operating at 10 kHz, recorded the corresponding time of the maximum value of the received signal and compared it with the predicted results using (18) with the results shown in Fig. 2. The inset (a) in Fig. 2 depicts the simulated received signal $y(t)$. Note that, the AWGN has zero mean and a RMS voltage of 30 mv. The distance between the laser radar and the target was 8.1 m. In the simulation, the visibility of the fog was ~300 m and the corresponding extinction and backscattering coefficient were 0.136 m^{-1} and 0.0031 $m^{-1}sr^{-1}$, respectively. The blue bar in the inset Fig. 2(b) is the statistical result of the simulation, which illustrates a good match with the predicted data (shown in red dots).

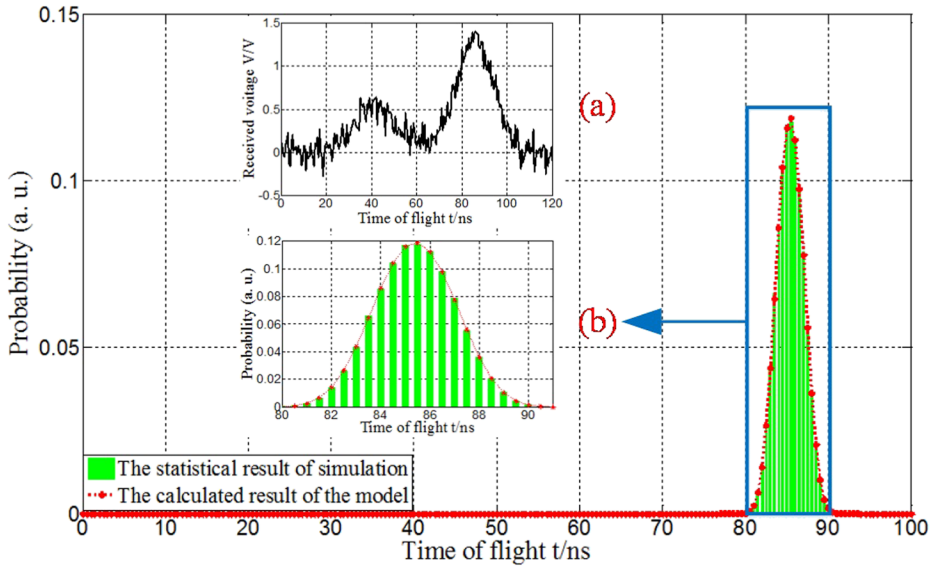

FIG. 2. The probability density distribution of ranging data obtained by the theoretical model and the simulation result.

IV. EXPERIMENT SETUP

Fig. 3(a) shows the schematic system block diagram of the proposed system, which is composed of the optical transmitter (Tx), optical Rx, indoor atmospheric chamber, and green laser. At the Tx we have used a semiconductor laser diode and an optical lens for compressing the output divergence angle. $l_1 = 0.5m$ is the span between the laser radar and the fog chamber, $l_2 = 5.5m$ is the chamber length, $l_3 = 2.1m$ is the distance between the fog chamber and the target. The atmospheric chamber with a dimension of $550 \times 30 \times 30cm^3$ was used in order to assess the link performance under fog conditions, see Fig. 3(b). The fog was generated using a commercial water vaporizing machine and injected into the chamber, where its density and movement were controlled using a number of fans

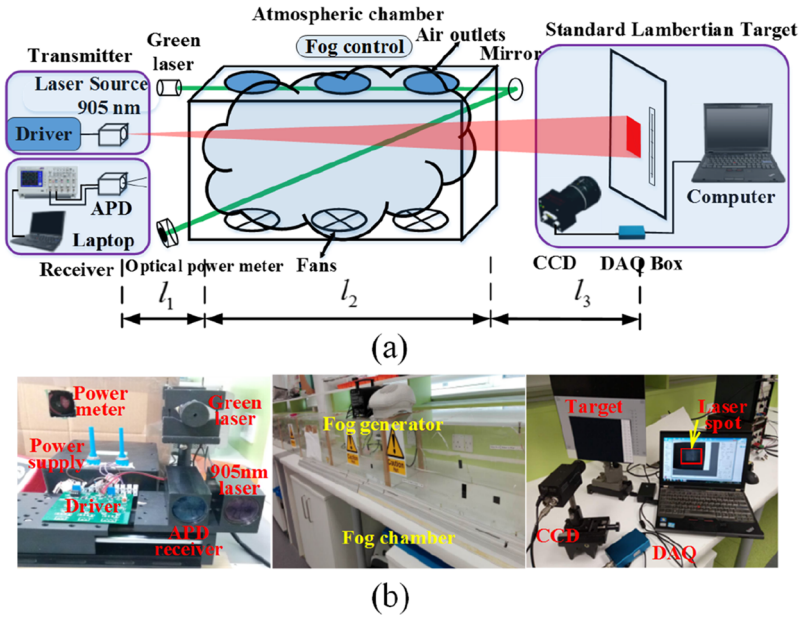

FIG. 3. The proposed ILR system working in the fog chamber: (a) schematic system block diagram, and (b) experimental setup.

and ventilation outlets as in Ref. 35. The output of the Rx, which is composed of a lens, an avalanche photodiode (APD) and a transconductance amplifier, was captured using a digital oscilloscope (Agilent DSO80604B) for offline processing using the LABVIEW. A green laser at λ of 543 nm and an optical power meter were used to measure the link visibility V to ensure a desirable correlation of the corresponding measured fog attenuations. However, under the homogenous fog condition (i.e., very small change in fog movement within the chamber) the fog induced attenuation is significant, which results in reduced V and ultimately a link failure. Doubling the propagation span within the chamber will compensate for the effect of small scale fluctuations, which optimizes the calculation of V and characterization of fog induced attenuation with improved accuracy.[25]

V. RESULTS AND DISCUSSIONS

In this section, we present both predicted and measured results on the effect of fog on PDD of $d_{ra}(t)$ of ILR. Using an indoor atmospheric chamber it is possible to create almost the same fog conditions under a highly controlled environment and carry out measurements repeatedly, which is not possible in outdoor environments due to changing weather conditions.[8] To ensure reliability and consistency of the results, each experiment was conducted five times. All the key system parameters adopted in this work are given in Table I.

A. The predicted PDD of ranging data under different fog intensities

In intensity modulation - direct detection FSO systems, the most important noise sources are the signal and ambient induced shot noises $n_{op}(t)$, dark current shot noise $n_{op}(t)$, and the electronic noise $n_{op}(t)$, which needs to be considered in ILR systems.[14] The received signal is given by:

$$S(t) = f(t) + n_{op}(t) + n_{dc}(t) + n_{ele}(t), \tag{19}$$

where $f(t)$ is the time-resolved output. Note that, the ambient induced noise can be reduced using an optical filter, and $n_{op}(t)$ can be ignored since the received optical signal is relatively large (i.e., high signal shot noise particularly when using APD). Under a relatively clear atmospheric channel condition (i.e., a high visibility V of > 5 km), the SNR is high compared to the channel with fog for both cases of a link with the shot noise limit, and shot noise plus the electrical noise limit. With fog, the intensity of received signal (i.e., pulse) drops, which results in an enhanced extinction coefficient. Here, we first determine $f(t)$ for a range of fog intensities using (13) and (14), and using (18) we obtain the PDD of $n_{op}(t)$ of ILR for a range of SNR.

Figs. 4–7 display PDDs of $d_{ra}(t)$ for ILR for a range of SNR (i.e., 1, 5, 15 and 30 dB) and received pulse width (FWHM), and $y_r(t)$ of Gaussian function, Parabolic function, and Heavy-tailed function.

TABLE I. The system structural parameters of the experiment laser radar.

System	Parameter	Value
Tx	Wavelength λ	905 nm
	Pulse peak power	70 W
	Transmitting efficiency	85 %
	Pulse width (FWHM)	20 ns
	Repetition frequency	10 kHz
	Horizontal irradiating FOV	8 mrad
	Vertical irradiating FOV	6.3 mrad
Target	Hemispherical reflectivity	15.75 %
Rx	Receiver aperture diameter	0.02 m
	Receiving efficiency	90 %
	Trans-conductance	10 kΩ
	Amplifier bandwidth	50 MHz
	Receiver FOV	12 mrad
	Filter bandwidth	50 nm
	Photodetector responsivity	0.56 A/W

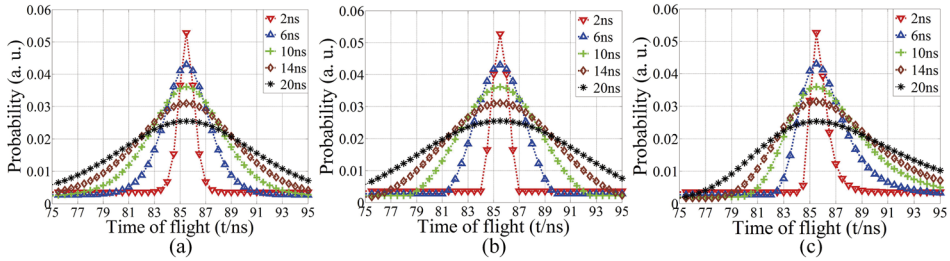

FIG. 4. The probability density distribution of $d_{ra}(t)$ of ILR under different fog intensities with SNR = 1dB, for a range of received pulse width (FWHM), and received pulse shapes of: (a) Gaussian function, (b) Parabolic function, and (c) Heavy-tailed function.

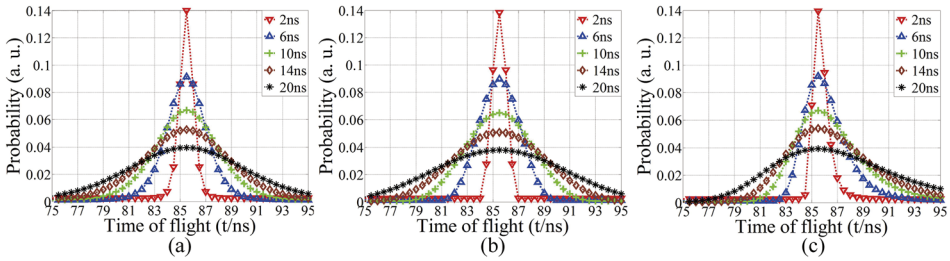

FIG. 5. The probability density distribution of $d_{ra}(t)$ of ILR under different fog intensities with SNR = 5dB, for a range of received pulse width (FWHM), and received pulse shapes of: (a) Gaussian function, (b) Parabolic function, and (c) Heavy-tailed function.

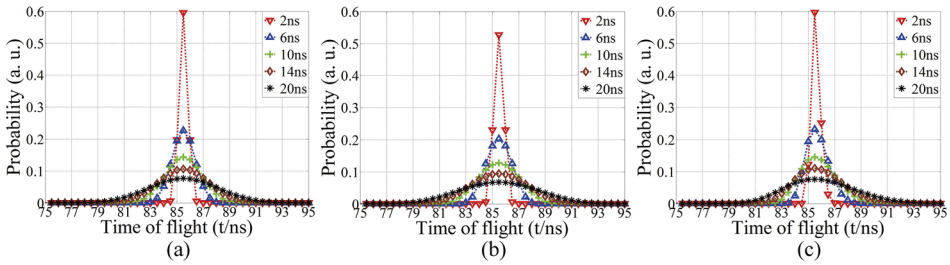

FIG. 6. The probability density distribution of $d_{ra}(t)$ of ILR under different fog intensities with SNR = 15dB, for a range of received pulse width (FWHM), and received pulse shapes of: (a) Gaussian function, (b) Parabolic function, and (c) Heavy-tailed function.

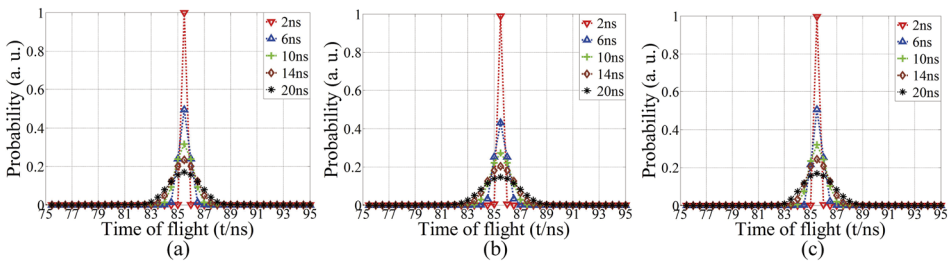

FIG. 7. The probability density distribution of $d_{ra}(t)$ of ILR under different fog intensities with SNR = 30dB, for a range of received pulse width (FWHM), and received pulse shapes of: (a) Gaussian function, (b) Parabolic function, and (c) Heavy-tailed function.

As can be observed from Figs. 4–7, the PDD spread out with increasing values of the pulse width. For a given received pulse width, PDD is more concentrated on the real value of the distance for higher values of SNR. E.g., for a Gaussian shaped received pulse with a FWHM of 2 ns, see Fig. 4–7(a), PDDs are very narrow, meaning that $d_{ra}(t)$ tend to be the actual distance value (i.e., 85.5 ns). Note that, at higher values of SNR PDDs are Gaussian for all the three $y_r(t)$. However, for lower SNRs (i.e., < 5 dB) the shape of PDD tends to be $y_r(t)$ with a wider width, thus indicating a reduced precision accuracy.

B. PDD of ranging data based on the approximate model with fogy

Although (18) can be used to determine accurately PDD of $d_{ra}(t)$ under fog conditions. However, it is difficult to obtain the exact result in a real time due to the complexity of the integral in (18). For low values of SNR, see Fig. 5, PDD of $d_{ra}(t)$ tends to be the same as $y_r(t)$. Here we take the approximate model based on the numerical calculation of (18) to determine the PDD as given by:

$$\begin{aligned} p(t) &= f(t-t_0)\cdot\rho(t-t_0) \\ &= \frac{1}{\sqrt{2\pi}\sigma_m} f(t-t_0) e^{-\left(\frac{t-t_0}{\sqrt{2}\sigma_m}\right)^2}, \end{aligned} \tag{20}$$

where $f(t-t_o)$ is the time-resolved output without noise of lidar system, which can be determined using (13). $\rho(t-t_o)$ is the modulated Gaussian function (MGF) with mean of zero and variance of σ_m.

In Fig. 8 we show the influence of SNR on the variance σ_m of MGF for a range of $y_r(t)$ width based on (20) and using the parameters given in the Section V A. As can be seen, all plots almost have the same profiles decreasing and increasing with the pulse width of $y_r(t)$ and SNR, respectively. Note that, here σ_m represent the dispersion experienced by $d_{ra}(t)$, and using the least square fitting it can be expressed as:

$$\sigma_m = ae^{b\varphi_{SNR}} + ce^{d\varphi_{SNR}}, \tag{21}$$

where a, b, c and d are the parameters relate to the width of $y_r(t)$, which are given in Table II along with the root mean square error (RMSE), and is the value of SNR.

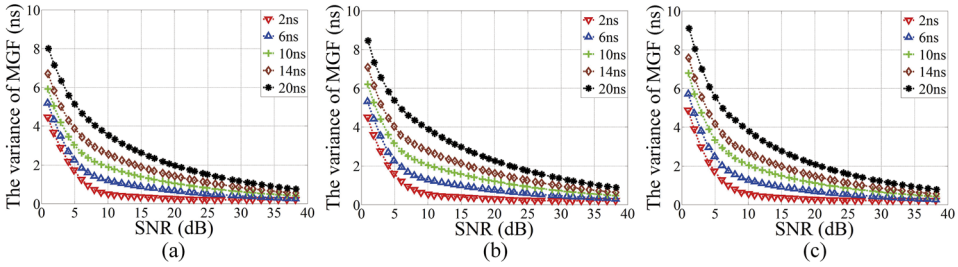

FIG. 8. The variance of MGF vs SNR for a range of received pulse width and pulse shapes of: (a) Gaussian function, (b) Parabolic function, and (c) Heavy-tailed function.

TABLE II. The parameters of Eq. (21).

	Gaussian pulse shape	Parabolic pulse shape	Heavy-tailed pulse shape
a	$-0.121\tau + 5.8$	$-0.105\tau + 5.75$	$-0.075\tau + 6.18$
b	$0.179\tau^{-0.807} - 0.374$	$-0.0367\tau^{0.567} - 0.25$	$0.139\tau^{-0.372} - 0.401$
c	$0.311\tau - 0.268$	$0.337\tau - 0.221$	$0.327\tau - 0.234$
d	$0.151\tau^{-1.42} - 0.057$	$0.087\tau^{-1.322} - 0.054$	$0.162\tau^{-1.81} - 0.055$
R^2	0.9871	0.9796	0.9802
RMSE	0.1326	0.1403	0.1385

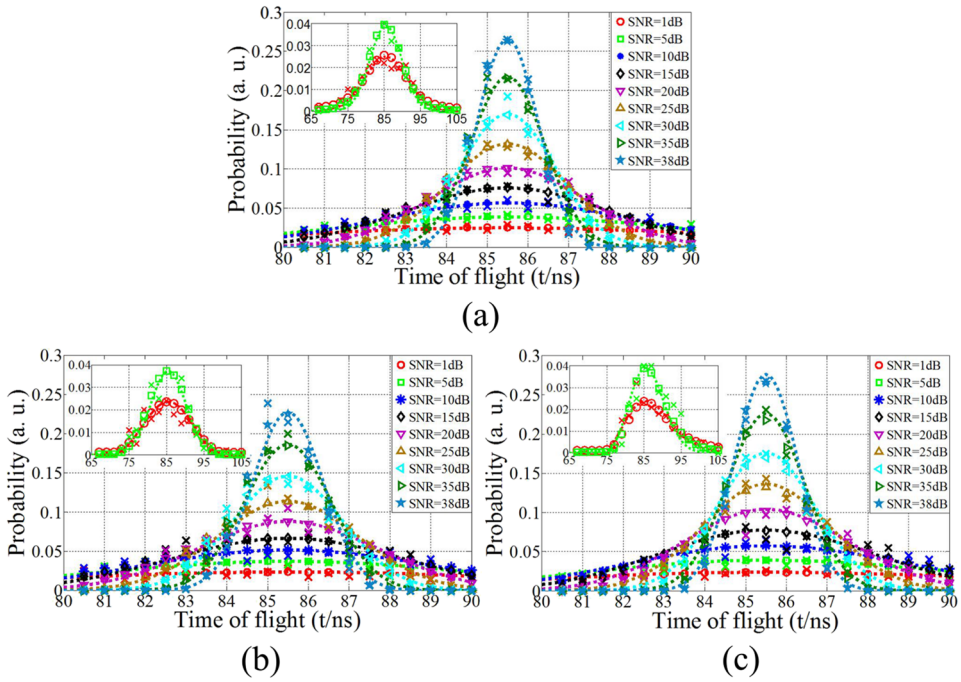

FIG. 9. The probability density distribution of $d_{ra}(t)$ of imaging laser radar under different fog intensity. The received pulse shape is: (a) Gaussian function, (b) Parabolic function, and (c) Heavy-tailed function.

C. The experimental result of PDD of ranging data under different fog intensity

The measured flight time of the laser pulse, which has a maximum detection probability, is ~85.5 ns. In our system the trigger delay of the circuit is ~31.5 ns, in this case, and the real received time is 54 ns. Therefore, the distance between the laser radar and the target is 8.1 m, which is the

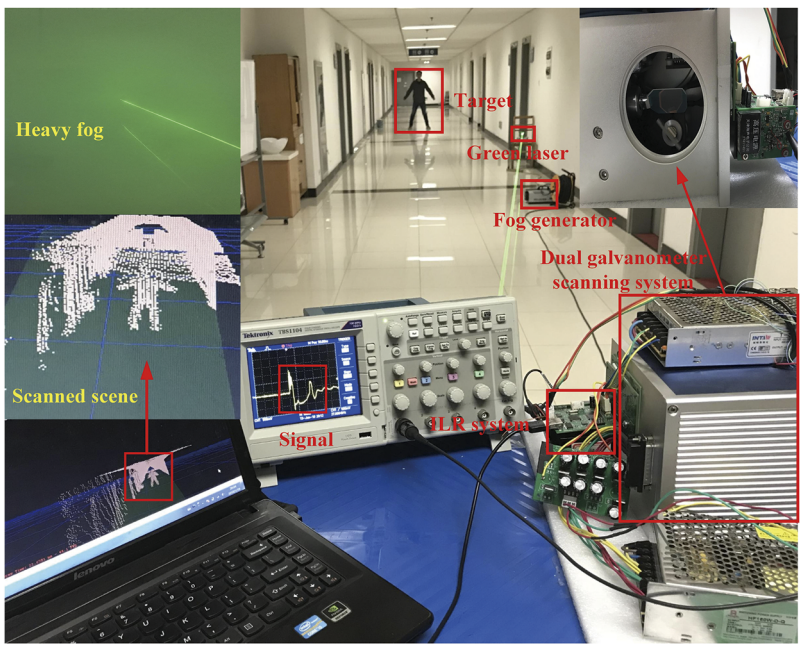

FIG. 10. The scanned scene of the ILR system with a dual galvanometer scanning system.

same as the experimental setup. The narrow and wide width of the probability density curve in Fig. 9 indicates higher and lower detection accuracies of $d_{ra}(t)$ for the laser radar, respectively.

Fig. 9 illustrate the predicted PDD of $d_{ra}(t)$ as a function of the time of flight for a range of SNR and for three different pulse shapes. The short dash line with the corresponding color is the predicted result using the approximate model (i.e., Eq. (20)). As can be observed, the approximate model match well with the accurate data (using Eq. (16)) near the target location, even at lower values of SNR (i.e., < 5 dB), the inset, with only minor differences at both rising and falling edges. Note that, for both Gaussian and parabolic pulse shapes the approximated model underestimates the accurate model slightly. However, for heavy-tailed $y_r(t)$, the approximated model slightly overestimates and underestimates the accurate model at rising and falling edges. The symbol "x" with the corresponding color in Fig. 9 show the statistical result for the experimental data. Using an Agilent oscilloscope (DSO80604B) and LABVIEW, we record the echo pulse 2000 times at each values of SNR and then determined the time of flight of $y_r(t)$ using the peak detection method. Note that, the experimental result match well with the accurate and approximated models within the error margin of < 1 %.

D. The PDD model used to improve the precision of target ranging and imaging

In order to evaluate the effectiveness of the proposed PDD model, which is used to improve the precision of target ranging and imaging, a dual galvanometer scanning system was adopted to obtain a 128×128 pixel resolution scanned scene, as shown in Fig. 10. We used a 42 m long corridor to test

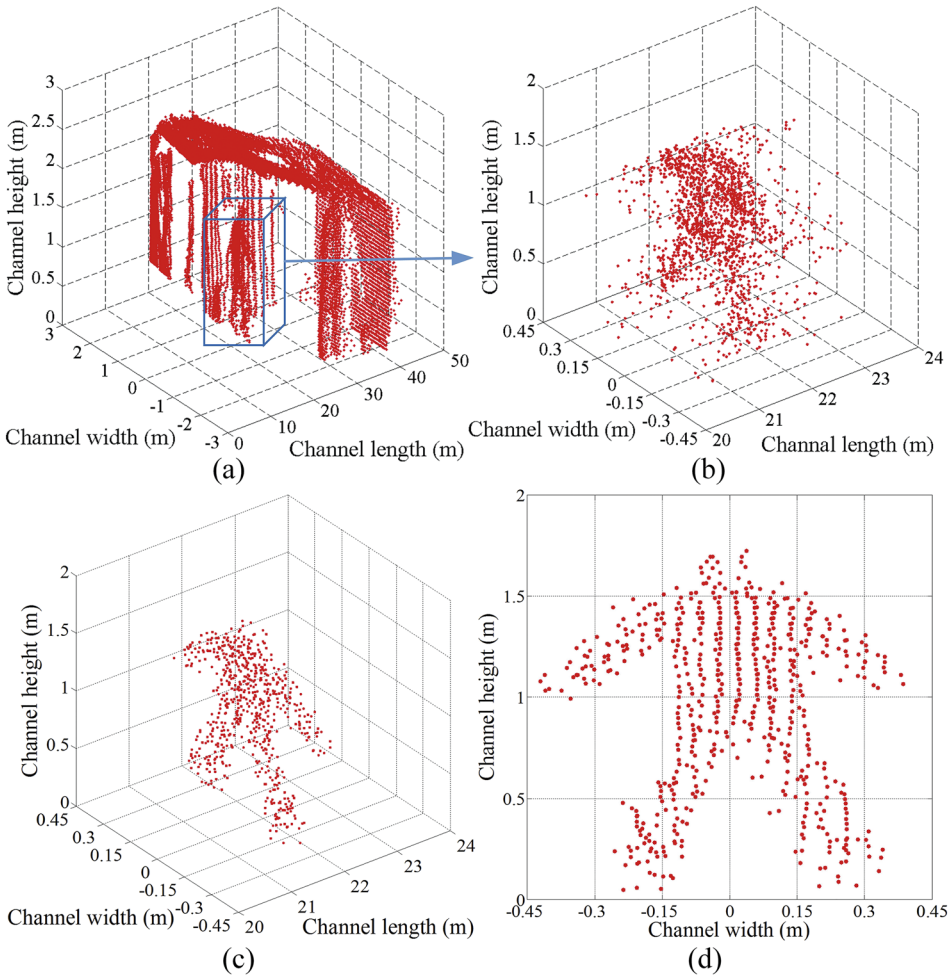

FIG. 11. The scanned scene of the target with a visibility of ~120 m and the SNR of the received signal tends to 5 dB.

the proposed system performance under fog conditions. Fog was generated using a commercial water vaporizing machine and its density and distribution were controlled using two large fans placed along the corridor. The target (a person with a 1.8 m height) was positioned 21.75 m away from the ILR system. The system key parameters are given in Table I. Here, a square wave signal was used to trigger the laser diode, which results in an output pulse with a Gaussian profile. Note that, by changing the trigger waveform and adjusting the parameters of the pulse shaping circuit the desired output pulse profiles can be obtained. Fig. 11(a) shows the scanned scene of the target under moderate fog (i.e., a visibility of ~120 m) and the SNR of 5 dB. Having determined the ranging distance l between the target and ILR, the specific coordinates of the target point can be obtained using the following equation:

$$\begin{pmatrix} x \\ y \\ z \end{pmatrix} = l * \begin{pmatrix} \sin\theta_s \cos\varphi_s \\ \sin\theta_s \sin\varphi_s \\ \cos\theta_s \end{pmatrix}, \tag{22}$$

where θ_s and φ_s are the scanning angles of the two mirrors for the dual galvanometer scanning system, respectively.

Note that, since there is no obstacles close to the target, the target can be separated from the scanned scene. As shown in Fig. 11(b), the depth of the target is within the range of 20 m to 24 m, which is considerably higher than the designed ranging accuracy of the ILR system of ±0.1 m. Note also that, the most important factor, which significantly affects the accuracy of target recognition, is fog. Here, we can use the priori estimation of PDD under fog conditions with a SNR of 5 dB, see Fig. 5. We assume that the ranging data obtained in Fig. 11(b) at each scanning point obey the priori estimation of PDD and therefore choose the value of the ranging distance with a maximum probability as the final value. Figs. 11(c) and (d) show the predicted result for the ranging data, with the depth scanning points of the target of 21.75 ± 0.15 m, which is slightly larger than the designed ranging accuracy but much lower than the original ranging data.

VI. CONCLUSION

In this paper, we demonstrated the impact of fog on the PDD of ranging data of the ILR system. A physical model of the reflected laser pulses due to a standard Lambertian target was introduced and based on this a theoretical model of PDD of ranging data was developed under different fog conditions. We showed that the simulation results are in a good agreement with the predicted model. Considering the complexity of the theoretical model, an approximate model was proposed to determine the PDD of ranging data. The approximate model showed that PDD can be expressed as a product of the received pulse function and the modulated Gaussian function, which is related to the width of received pulse and the SNR. We showed that measured ranging data using ILR under fog conditions matched well with the both the exact and approximate models within the margin of error of < 1 %. The results reported can be used to offer a priori estimation of PDD of a laser radar under fog conditions and improve the precision of target ranging and imaging.

ACKNOWLEDGMENTS

This research was supported by Nanjing University of Science and Technology in China and University of Northumbria, Newcastle upon Tyne, UK. We thank the Northumbria Communications Research Laboratory for the use of their equipment.

National Natural Science Foundation of China (61371167).

[1] M. A. Albota, R. M. Heinrichs, D. G. Kocher, D. G. Fouche, B. E. Player, M. E. O'Brien, B. F. Aull, J. J. Zayhowski, J. Mooney, B. C. Willard, and R. R. Carlson, "Three-dimensional imaging laser radar with a photon-counting avalanche photodiode array and microchip laser," Appl. Optics **41**, 7671 (2002).

[2] K. Bers, K. R. Schulz, and W. Armbruster, "Laser radar system for obstacle avoidance," Proc. SPIE **5958** (2005), Lasers and Appl.

[3] M. M. Kleiman and N. Shiloah, "The effect of dense atmospheric environment on the performances of laser radar sensors used for collision avoidance," Proc. SPIE **3707**, 624–635 (1999), Laser Radar Tech. and Appl. IV.

[4] H. N. Burns, C. G. Christodoulou, and G. D. Boreman, "System design of a pulsed laser rangefinder," Opt. Eng. **30**, 323 (1991).

[5] E. W. Eloranta, "Pratical model for the calculation of multiply scattered lidar returns," Appl. Opt. **37**, 2464 (1998).
[6] Y. Yang, M. Mandehgar, and D. R. Grischkowsky, "Broadband THz signals propagate through dense fog," IEEE Photonics Technology Letters **27**, 383 (2015).
[7] Y. Yang, M. Mandehgar, and D. Grischkowsky, "Time domain measurement of the THz refractivity of water vapor," Optics Express **20**, 26208 (2012).
[8] Z. Ghassemlooy, W. Popoola, and S. Rajbhandari, *Optical Wireless Communications – System and Channel Modelling with Matlab*, CRC Publisher, USA, August 2012, ISBN: 978-4398-5188-3.
[9] M. A. Naboulsi, H. Sizun, and F. Fornel, "Fog attenuation prediction for optical and infrared waves," Opt. Eng. **43**, 319 (2004).
[10] R. Nebuloni, "Empirical relationships between extinction coefficient and visibility in fog," Appl. Opt. **44**, 3795 (2005).
[11] M. Grabner and V. Kvicera, "The wavelength dependent model of extinction in fog and haze for free space optical communication," Opt. Exp. **19**, 3379 (2011).
[12] M. Ijaz, Z. Ghassemlooy, J. Pesek, O. Fiser, H. L. Minh, and E. Bentley, "Modeling of fog and smoke attenuation in free space optical communications link under controlled laboratory conditions," J. Lightw. Technol. **31**, 1720 (2013).
[13] M. Grabner and V. Kvicera, "Multiple scattering in rain and fog on free-space-optical links," J. Lightw. Technol. **32**, 513 (2014).
[14] *Optical Wireless Communications – An Emerging Technology*, edited by M. Uysal, C. Capsoni, Z. Ghassemlooy, A. C. Boucouvalas, and E. G. Udvary (Springer, 2016).
[15] L. Jiancheng, J. Haijiao, Y. Wei, W. Chunyong, and L. Zhenhua, "Range uncertainty distribution of direct-detection laser radar with a peak-detecting routine," Optik-International Journal for Light and Electron Optics **124**, 5202 (2013).
[16] F. Taillade1, E. Belin, and E. Dumont, "An analytical model for backscattered luminance in fog: Comparisons with Monte Carlo computations and experimental results," Meas. Sci. Tech. **19**, 055302 (2008).
[17] J. W. Giles, I. N. Bankman, R. M. Sova, T. R. Morgan, D. D. Duncan, J. A. Millard, W. J. Green, and F. J. Marcotte, "Lidar system model for use with path obscurants and experimental validation," Appl. Opt. **47**, 4085 (2008).
[18] S. Y. Chua, X. Wang, N. Guo, and C. S. Tan, "Influence of target reflection on three-dimensional range gated reconstruction," Applied Optics **55**, 6588 (2016).
[19] C. Grönwall, O. Steinvall, F. Gustafsson, and T. Chevalier, "Influence of laser radar sensor parameters on range-measurement and shape-fitting uncertainties," Optical Engineering **46**, 106201 (2007).
[20] S. Johnson, T. Nichols, P. Gatt, and T. Klausutis, "Range precision of direct detection laser radar systems," Proc. SPIE **5412**, 72–86 (2004).
[21] B. T. N. Evans, "Sensitivity of the backscatter/extinction ratio to changes in aerosol properties: Implications for lidar," Appl. Opt. **27**, 3299 (1988).
[22] V. A. Kovalev, "Lidar measurement of the vertical aerosol extinction profiles with range-dependent backscatter-to-extinction ratios," Appl. Opt. **32**, 6053 (1993).
[23] H. R. Carlon, D. H. Anderson, M. E. Milham, T. L. Tarnove, R. H. Frickel, and I. Sindoni, "Infrared extinction spectra of some common liquid aerosols," Appl. Opt. **16**, 1598 (1977).
[24] H. C. van de Hulst, *Light Scattering by Small Particles* (Dover Publications, New York, 1981).
[25] W. Song, Z. Ghassemlooy, J.-C. Lai *et al.*, "The irradiating field of view of imaging laser radar under fog conditions in a controlled laboratory environment," Journal of Optics **19**, 045605 (2017).
[26] M. Ijaz, Z. Ghassemlooy, S. Rajbhandari, H. L. Minh, J. Perez, and A. Gholami, "Comparison of 830 nm and 1550 nm based free space optical communications link under controlled fog conditions," IEEE 8th CSNDSP Int. Symposium, 2012.
[27] R. G. Eldridge, "Haze and fog aerosol distributions," J. Atmos. Sci. **23**, 605 (1966).
[28] C. F. Bohren and D. R. Huffman, *Absorption and scattering of light by small particles* (John Wiley & Sons, 2008).
[29] J. Redemann *et al.*, "Retrieving the vertical structure of the effective aerosol complex index of refraction from a combination of aerosol in situ and remote sensing measurements during TARFOX," J. Geo. Res. **105**, 9949, https://doi.org/10.1029/1999jd901044 (2000).
[30] L. C. Andrews and R. L. Phillips, *Laser beam propagation through random media* (SPIE Press, Bellingham, WA, 2005), Vol. PM152.
[31] R. M. Measures, *Laser Remote Sensing: Fundamentals and applications* (Krieger, 1992).
[32] S. Cain, R. Richmond, and E. Armstrong, "Flash light detection and ranging range accuracy limits for returns from single opaque surfaces via Cramer-Rao bounds," Applied Optics **45**, 6154 (2006).
[33] O. Steinvall, "Effects of target shape and reflection on laser radar cross sections," Applied Optics **39**, 4381 (2000).
[34] O. Kallenberg, *Foundations of modern probability* (Springer Science & Business Media, 2006).
[35] M. Ijaz, "Experimental characteristics and modelling at atmospheric fog and turbulence in FSO," Ph. D dissertation, Dept. Elect. Eng., Univ. of Northumbria, Newcastle, UK, 2013.